GeoConvention 2015
GEOSCIENCE
new horizons
Telus Convention Centre • 4-8 May 2015 • Calgary, AB Canada

Lowrank RTM for converted wave imaging

Lorenzo Casasanta[*]*(CGG), Zhiguang Xue (UT Austin), Sam Gray (CGG)*

Summary

This paper is an attempt to fill the technology gap existing between pure P- and PS-wave imaging. Full wavefield extrapolation techniques are well developed for P-wave and RTM has been now available for almost a decade. Conversely, ray based migration algorithms are still the workhorse for converted-wave (PS-wave) depth imaging. Here, we introduce a new converted-wave anisotropic RTM, using a low-rank decomposition of mixed-domain space-wavenumber propagators for quasi-P and quasi-S waves. These operators are formal integral solutions of the pure-mode wave equations which guarantee stable and dispersion-free time extrapolation for coarse time steps in anisotropic, heterogeneous media. The pure-mode extrapolators are attractive for both PS-wave structural imaging and velocity analysis. An ocean bottom cable synthetic example illustrates the effectiveness of low-rank PS-wave RTM when compared against state-of-the-art Gaussian beam and finite difference RTM algorithms.

Introduction

Multicomponent Kirchhoff migration remains the workhorse for converted-wave (PS-wave) depth imaging. Recently, Casasanta and Gray (2014) extended Gaussian-beam migration (GBM) to PS-wave imaging. However, neither full elastic nor PS-wave reverse-time migration (RTM) have seen widespread use in practice, despite promising research over the last decade (Sun et al., 2006; Cheng et al. 2014). This is at least in part because popular finite difference (FD) solvers for both the elastic wave equation and (quasi-P and quasi-S, or qP and qS) wave equations suffer from both computational and algorithmic shortcomings.

From a computational standpoint, a fourth order FD stencil imposes either: dense grid spacing for non-aliased slow S-wave extrapolation; or small time steps for stable fast P-wave propagation (Soubaras and Zhang, 2008). These constraints significantly increase the computational cost of both full elastic and PS-wave RTM compared to P-wave RTM.

From an algorithmic standpoint, anisotropic elastic wave-extrapolators support the propagation of coupled P- and S-wave modes which can be decoupled using a generalization of the Helmoltz vector decomposition (Yan and Sava, 2011). On a realistic 3D-survey this procedure is I/O intensive, as the operators involved are space-variant. Although more efficient implementations are emerging (Cheng and Fomel, 2014), elastic wave mode separation still assumes accurate knowledge of the elastic-coefficient tensor, which is unlikely in early stages of depth imaging projects. Failure in wavefront separation will increase the amount of intra-modal cross-talk noise, possibly to the point of questioning the advantages of full-wavefield imaging over ray-based methods.

For anisotropic P-wave RTM, the standard propagator is a FD solution of a pseudo-acoustic wave equation for transverse isotropic or orthorhombic media with arbitrarily oriented symmetry axis. In such formulation, S-wave velocity along the symmetry axis is set to zero $(V_{S0}=0)$, ensuring stable P-wave propagation in an energy bounded system as long as anisotropy parameters satisfy $\varepsilon \geq \delta$. Any residual S-wave energy is generally weak and easy to remove before or after imaging. The analogous solution for anisotropic S-wave FD propagators is not practical because the energy constraint for the pseudo-acoustic S-wave extrapolator requires $\varepsilon \leq \delta$ (Zhang et al., 2011), which is not realistic for typical rock properties.

In this paper, we propose using mixed-domain (space/wavenumber) operators (Wards et al., 2008).

These spectral operators implement analytical integral solutions of the scalar wave equations (Etgen and Brandsberg-Dahl, 2009; Fowler et al., 2010). These are suitable for PS-wave structural imaging and velocity analysis because they propagate pure-mode, dispersion-free qP- and qS-wavefields, and they are stable for large time steps, even (though impractical) beyond the Nyquist limit (Fowler et al., 2010). Further, the original space-wavenumber content of the wavefields is approximated to a desired accuracy by a lowrank decomposition (Fomel et al., 2013) which makes the wave-extrapolation feasible and accurate for practical application. We have implemented a PS-wave RTM using mixed-domain extrapolators based on exact dispersion relation in TI media. We present an ocean bottom cable (OBC) synthetic example to illustrate the effectiveness of this low-rank PS-wave RTM when compared against state of the art Gaussian beam (GBM) and pseudo-acoustic FD RTM algorithms in heterogeneous TTI media.

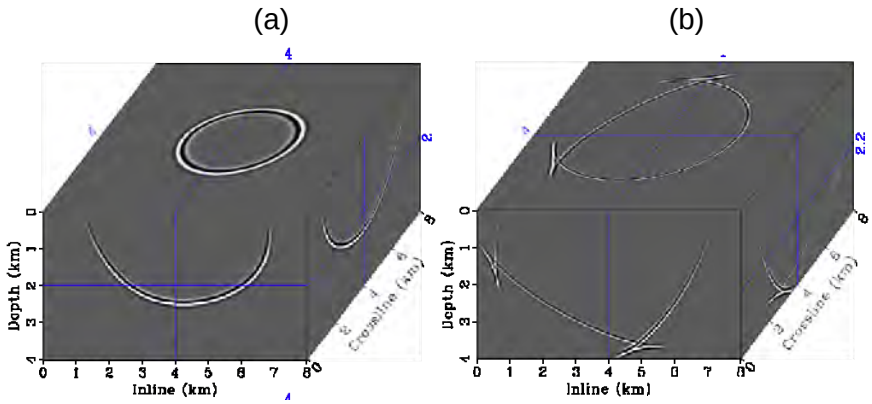

Figure 1: *Mixed-domain P- (a) and SV- (b) lowrank extrapolation snapshots in a constant 3D TI medium.* V_{P0}/V_{S0} =2.41, ε=.25, δ=.01, ϑ=30^0, φ=0^0.

Method

Let $p(\mathbf{x},t)$ satisfy a scalar (P or S) wave equation in an inhomogeneous anisotropic medium described by its phase velocity $V(\mathbf{x},\mathbf{k})$, which depends on space $\mathbf{x}$ and wave vector $\mathbf{k}$. The wavefield at the next time step $t+\Delta t$ can be approximated by the mixed domain operator (Wards et al., 2008)

$$p(\mathbf{x},t+\Delta t) \cong \int d\mathbf{k}\, e^{i\phi(\mathbf{x},\mathbf{k},\Delta t)}\, P(\mathbf{k},t), \tag{1}$$

where *P*(**k**,*t*) is the spatial Fourier transform of the wavefield $p(\mathbf{x},t)$ at time step t and $\phi(\mathbf{x},\mathbf{k},\Delta t)$ is the mixed-domain phase function. In the high-frequency limit and for a smooth phase velocity function, a first order Taylor expansion approximates $\phi(\mathbf{x},\mathbf{k},\Delta t) \cong \mathbf{k}^T\mathbf{x} + V(\mathbf{x},\mathbf{k})|\mathbf{k}|\Delta t$ (Fomel et al., 2013). The recursion in equation 1 is unconditionally stable for constant or smoothly varying velocity models (Ying and Sun,2014). However, an analysis like that of Etgen (1994) is needed to assess the stability of equation 1 for complicated subsurface models. Finally, two complex-valued one-step operators in equation 1 can be combined to obtain the real-valued two-step operator (Etgen and Brandsberg-Dahl, 2009; Soubaras and Zhang, 2008) The computational cost for a straightforward application of equation 1 is $O(N_{\mathbf{x}}^2)$, where $N_{\mathbf{x}}$ is the total size of the three-dimensional $\mathbf{x}$ grid. For fixed Δt, a lowrank r_ε approximation decomposes the wave extrapolation matrix into a separated representation with desired tolerance ε (Fomel et al., 2013):

$$W(\mathbf{x},\mathbf{k}) = e^{i[\phi(\mathbf{x},\mathbf{k},\Delta t)-\mathbf{k}^T\mathbf{x}]} \cong \sum_{m=1}^{M}\sum_{n=1}^{N} W(\mathbf{x},\mathbf{k}_m)\, a_{mn}\, W(\mathbf{x}_n,\mathbf{k}) \tag{2}$$

Using representation 2, the computation in equation 1 corresponds to the evaluation of $M = N = r_\varepsilon$ inverse FFTs with a cost of $O(MN_{\mathbf{x}}\log N_{\mathbf{x}})$ per time step, where r_ε is generally a small number for the oscillatory kernel in equation 2. Differently from SVD, lowrank decomposition evaluates a set of N representative spatial location (rows) and M representative wavenumbers (columns) without requiring knowledge of the whole matrix in equation 2.

Scalar PS-wave RTM requires the forward and backward time extrapolation of P- and S-wavefields injected at source and recording locations respectively. To this purpose we have designed mixed-domain P- and SV-wave matrices using equation 2 and the exact formulation for phase velocity $V(\mathbf{x},\mathbf{k})$ in a TI medium (Casasanta and Gray 2014):

$$2V_{P,SV}^2(\mathbf{x},\mathbf{k}) = V_{P0}^2\left[2(1-f)|\mathbf{k}|^2 + f|\mathbf{k}|^2 + 2\varepsilon k_{r0}^2 \pm \sqrt{(f|\mathbf{k}|^2 + 2\varepsilon k_{r0}^2)^2 - 8f(\varepsilon-\delta)k_{n0}^2 k_{r0}^2}\right] \quad (3)$$

where δ and ε are Thomsen parameters and $f = 1 - V_{S0}^2/V_{P0}^2$ depends on qP- and qSV-wave velocities. The sign of the square root gives the qP- (+) or the qSV- (-) wave phase velocity. The normal $\mathbf{k}_{n0} = (\mathbf{k}^T\mathbf{c})\mathbf{c}$ and radial $\mathbf{k}_{r0} = \mathbf{k} - \mathbf{k}_{n0}$ wavenumbers are the $\mathbf{k}$ projection parallel and orthogonal to the symmetry axis $\mathbf{c}$. Figure 1 shows (a) qP- and (b) qSV-wavefield snapshots computed using a two-step lowrank wave extrapolator in a constant TI medium. The time-step size is Δt=5 ms and the spatial grid sizes in (*x, y, z*) are all $\Delta\mathbf{x}$=20 m for both qP- and qSV-wave extrapolation. Since the model is homogeneous, the rank is 1 for the lowrank decomposition. The qP-wavefield slices are anelliptical, and the qSV-wavefield accurately produces the triplication in the wave surface. Neither qP- nor qSV-wavefield contains coupled modes.

Example

We discuss image quality and computational performance achieved by lowrank PS-wave RTM using a 2D OBC synthetic dataset recorded on a sloping seafloor at approximately 1.2 km depth, with shots near the sea surface. Shot and receiver sampling are 25 m and 100 m, respectively. The subsurface structure is complex, including high shallow $V_{P0}/V_{S0} \sim 5$ and a salt body with rough topography. The input data spectrum was limited to 20 Hz. The grid spacings in (*x, y, z*) were equal. However, we used different grids to propagate the qSV- and qP-wavefields ($\Delta\mathbf{x}_S$=12.5 m and $\Delta\mathbf{x}_P$=2$\Delta\mathbf{x}_S$) as well as different time steps (Δt_S=2Δt_P). In different experiments, we varied the length of the time step Δt_S from 2 ms to 8 ms while keeping the rank roughly the same (*M=N=18*), producing a range of errors in equation 3. Figure 2e-f shows the results obtained using the least accurate approximation (i.e., largest error) for the mixed-domain qP- and qSV-wave matrix $W(\mathbf{x},\mathbf{k})$. These results highlight the areas of most interest and challenge: steep TOS left flanks (Figure 2a-c-e) and subsalt reservoir sediments (Figure 2b-d-f).

We observed mild amplitude differences compared to the most accurate solution (smallest error) whilst the kinematics are essentially unaffected; the computation time gain was approximately a factor of two. Our lowrank RTM implementation (Figure 2e-f) generally outperformed the state-of-the art PS-wave GBM (Figure 2a-b) and quasi-acoustic FD RTM (Figure 2c-d). The steep shallow top of salt on our lowrank RTM (yellow arrows in Figure 2a-c-e) is more evident, although GBM shows cleaner sediments because of an imposed maximum-dip limitation of 70^o which is missing in both FD and lowrank RTM. Conversely, GBM is unable to reproduce all the branches of the subsalt PS-wave propagation, and fails to image the deeper sediments as completely as RTM (Figure 2b). In the same area the FD RTM image (Figure 3d) is not as complete as the lowrank RTM image (Figure 3f). In fact, as we mentioned before, the qSV FD RTM extrapolator requires $\varepsilon \le \delta$, which introduces an error in the S-wavefield kinematics away from the symmetry axis. This error is most evident on the steep shallow salt flanks and deeper subsalt sediments.

Conclusions

We have presented a novel PS-wave RTM implementation based on a lowrank approximation of the space-wavenumber mixed-domain wavefield extrapolator. Compared to FD RTM, the algorithm is attractive for scalar PS-wave imaging and velocity analysis because: (1) it is dispersion-free, with greater accuracy at high wavenumbers; (2) it is stable for large time steps, even beyond the Nyquist limit; (3) it propagates qP- and qS-waves with exact kinematics; (4) it offers direct control on the accuracy-efficiency trade-off by controlling the rank of the approximation in equation 3. We speculate that RTM using lowrank wavefield extrapolation can become a technology of choice for high-fidelity PS-wave imaging.

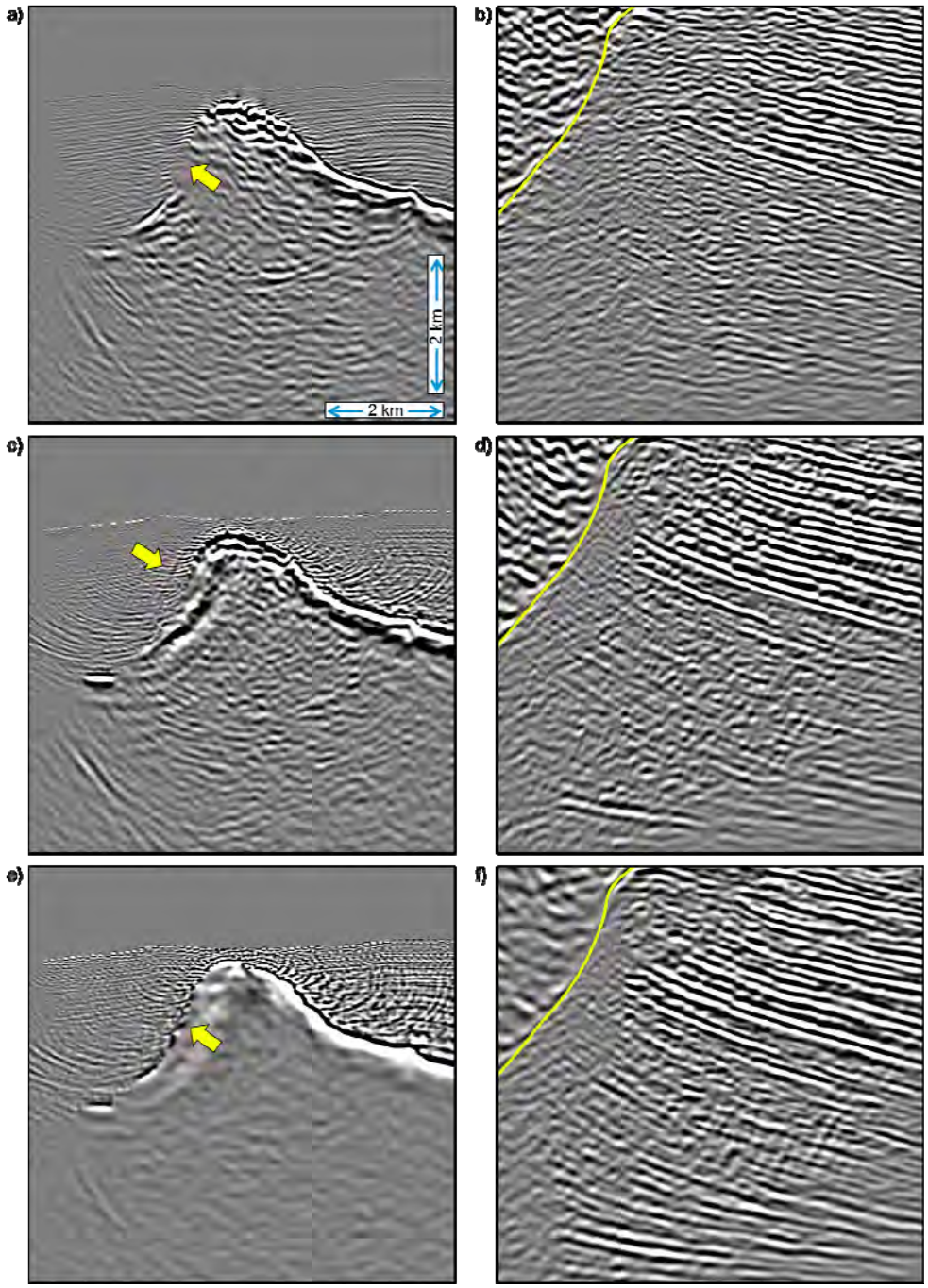

Figure 2 *OBC 2D synthetic PS-wave migration: CBM (a-b), FD RTM (c-d) and lowrank one-step RTM (e-f). (a-c-e): steep TOS left flanks. (b-d-f): subsalt reservoir sediments. The low-rank RTM results shows superior image quality and resolution particularly in the subsalt.*

Acknowledgements

We thank Chevron for providing the PS synthetic dataset. We also thank Sergey Fomel, Junzhe Sun, Botao Qin, Daniel Trad and Kristof De Meersman for stimulating discussions and critiques.

References

Casasanta, L., and Gray S. [2014], Converted-wave Gaussian-beam migration for sparse source or receivers: Geophysical Prospecting*, accepted for publication.*

Cheng, J., and Fomel, S, [2014], Fast algorithms of elastic wave mode separation and vector decomposition using low-rank approximation for anisotropic media : Geophysics, **79**, no. 4, C97–C110,

Cheng, J., Wu, Z., and Alkhalifah, T. [2014], Simulating propagation of decomposed elastic waves using low-rank mixed-domain integral operators for heterogeneous TI media: *84th Annual Meeting, SEG, Expanded Abstracts,* 3393-3399

Etgen, J., and Brandsberg-Dahl, S. [2009], The pseudo-analytical method: Application of pseudo-Laplacians to acoustic anisotropic wave propagation: *79th Annual Meeting, SEG, Expanded Abstracts,* 2552-2556*.*

Etgen , J. [1994] Stability of explicit depth extrapolation through laterally-varying media. SEG Technical Program Expanded Abstracts 1994,1266-1269.

Fomel, S., Ying, L., and Song, X. [2013], Seismic wave extrapolation using lowrank symbol approximation: Geophysical Prospecting*,* **61***,* 526-536*.*

Fowler, P. J., Du, X., and Fletcher, R.P., [2010b], Recursive integral time extrapolation methods for scalar waves: 80th Annual International Meeting, SEG, Expanded Abstracts, 3210–3215.

Sun, R., McMechan, Lee, G.A., Chow, C.J., and Chen. C., [2006]. Prestack scalar reverse-time depth migration of 3D elastic seismic data: Geophysics, **71***,* S199-207*.*

Sun, J., and Fomel, S. [2013], Lowrank one-step wave extrapolation: *83rd Annual International Meeting, SEG, Expanded Abstracts,* 3905-3910*.*

Soubaras, R., and Zhang , Y., [2008], Two-step explicit marching method for reverse time migration: 78th Annual International Meeting, SEG, Expanded Abstracts, 2272-2276.

Wards, B.D., Margrave, G.F., and Lamoureux, M.P., [2010], Phase-shift time stepping for wavefield propagation: *80th Annual International meeting, SEG, Expanded Abstracts,* 2988-2992*.*

Yan, J., and Sava, P., [2011], Elastic wave-mode separation for TTI media: Geophysics, **76**, no. 4, T65-T78,

Ying, L., Y. and Sun, J. [2014], Personal communication.

Zhang, Y., Zhang, H., and Zhang, G, [2011]. A stable TTI reverse time migration and its implementation. Geophysics **76**, WA3-WA11.